J. Fluid Mech. (2007), *vol.* 585, *pp.* 469–485.
doi:10.1017/S0022112007006921 Printed in the United Kingdom

Rough-wall boundary layers: mean flow universality

IAN P. CASTRO

School of Engineering Sciences, University of Southampton, Highfield, Southampton SO17 1BJ, UK
i.castro@soton.ac.uk

(Received 14 December 2006 and in revised form 2 May 2007)

Mean flow profiles, skin friction, and integral parameters for boundary layers developing naturally over a wide variety of fully aerodynamically rough surfaces are presented and discussed. The momentum thickness Reynolds number Re_θ extends to values in excess of 47 000 and, unlike previous work, a very wide range of the ratio of roughness element height to boundary-layer depth is covered ($0.03 < h/\delta < 0.5$). Comparisons are made with some classical formulations based on the assumption of a universal two-parameter form for the mean velocity profile, and also with other recent measurements. It is shown that appropriately re-written versions of the former can be used to collapse all the data, irrespective of the nature of the roughness, unless the surface is very rough, meaning that the typical roughness element height exceeds some 50 % of the boundary-layer momentum thickness, corresponding to about $h/\delta \gtrsim 0.2$.

1. Introduction and background

There is a substantial literature on rough-wall flows. In recent years, attention has concentrated on the extent to which the turbulence structure in the outer region, be it a boundary layer or a channel flow, differs from that of smooth-wall flows. Jiménez (2004) argues that provided the roughness element height h is below some 2–3 % of the boundary-layer thickness δ, there are no differences and, in line with classical thinking (e.g. Townsend 1976), the roughness acts merely to increase the surface stress, without causing structural changes in the flow. There is some evidence that this may not be entirely accurate (e.g. Krogstad, Antonia & Browne 1992) and it certainly cannot be the case once h/δ is sufficiently large. However, there is little extant work aimed at assessing the nature of the structural changes which must then occur, or even to determine the critical h/δ at which such changes begin and whether that critical h/δ depends on the nature of the roughness. What is more surprising, however, is that although there have been a number of attempts to develop useful correlations relating the surface friction to boundary-layer parameters over a wide range of surface roughness types (e.g. Mills & Hang 1983; Acharya, Bornstein & Escudier 1986; Granville 1987), such correlations have almost always considered only small h/δ and it is not known how adequate they are at larger values. The major exception, at least for fully three-dimensional roughness, seems to be the early work of Hama (1954) who, on the basis of studies of flow over wire meshes covering a wide range of scales, concluded that 'the long-conjectured universality of the roughness effect regardless of outside flow conditions has now been substantiated – at least for the case of fully developed roughness action at zero pressure gradient.' One might expect the mean flow to be more resilient than the turbulence structure, so that even

when h/δ is sufficiently large for changes to occur in the latter, the former might well retain a more classical behaviour. Although he did not state it explicitly, it can be deduced from Hama's paper that the maximum h/δ reached was somewhere in the range 0.3–0.5. With the hindsight of half-a-century, it is evident that this now classical work has some major shortcomings (see below), not least in that only a single roughness geometry was tested, but the resulting correlations have been the basis of a number of works since. It is the intention here to show that despite the deficiencies in the data, Hama's overall conclusion is valid for a wide variety of roughness geometries and that appropriate formulations of some of the later classical mean flow correlations are very resilient and thus provide useful results for surprisingly large h/δ. A careful reading of some of the more recent literature suggests that some of the lessons of the 1950s and 1960s have been forgotten and we therefore begin with a brief review of mean flow formulations and some of the more modern extant data.

The effect of surface roughness on the boundary-layer mean velocity profile is classically expressed using a roughness function ΔU^+, which modifies the usual smooth-wall formulation, as expressed below for the fully rough case,

$$u^+ \equiv \frac{U}{u_\tau} = \frac{1}{\kappa} \ln\left(\frac{(y-d)u_\tau}{\nu}\right) + A - \Delta U^+(h^+), \tag{1.1}$$

in the usual notation, but with inclusion of a zero plane displacement, d. For a smooth wall this would be zero, unless during the experiments the measured wall-distance was in error by some small amount. (The expected conformity with the smooth-wall version of (1.1) is sometimes used to deduce this error.) For a rough wall, with y measured from the bottom of the roughness elements, d can be interpreted as the effective height of momentum extraction and is always less than h. Jackson (1981) has shown that this height – essentially the height at which the mean surface drag appears to act – is implicit in the derivation of the log law. In general, ΔU^+ is a function of h^+ and the geometrical parameters defining the element shapes and arrangement – what we might call the roughness texture. In (1.1), we limit this dependence to element height, h. The alternative way of expressing the rough-wall profile in cases of fully rough surfaces (when viscous effects at the the surface are negligible), favoured by the meteorological community for whom fully rough conditions almost always pertain, is to write

$$u^+ \equiv \frac{U}{u_\tau} = \frac{1}{\kappa} \ln\left(\frac{y-d}{y_0}\right). \tag{1.2}$$

y_0 is the roughness length, which embodies the effect of the roughness function in (1.1) and is determined by h and the roughness texture alone. ΔU^+ and y_0 are simply alternative, but entirely equivalent, measures of the roughness and are related via

$$\Delta U^+ = A + \frac{1}{\kappa}\ln(Re^*) \equiv A + \frac{1}{\kappa}\ln(h^+) + \frac{1}{\kappa}\ln\left(\frac{y_0}{h}\right), \tag{1.3}$$

where Re^* is the roughness Reynolds number, $y_0 u_\tau/\nu$, which must usually exceed at least $O(1)$ for fully rough conditions to exist – i.e. for viscous effects to be negligible (Snyder & Castro 2002). In their review, Raupach, Antonia & Rajagopalan (1991) brought together a wide body of data from both the engineering and the meteorological communities. Following most authors, they characterized the effect of roughness by plotting ΔU^+ *vs.* h^+. This clearly shows the expected increase in ΔU^+ with increasing h^+ for each type of roughness, as implied by (1.3), but does not collapse all the data since y_0 and thus y_0/h is in principle a function of all the features

of the roughness geometry (as also, incidentally, is d/h). Attention is concentrated in this paper on fully rough cases, where viscous scales such as ν/u_τ are not relevant, so we use (1.2) and thus y_0 as the appropriate scale defining the roughness (rather than h^+). We are not concerned here with the nature of the relationship between geometry and the resulting y_0 (but see the Jiménez 2004 and Raupach *et al.* 1991 reviews for some examples of such work).

The profile expressions above can be modified to include the outer flow, usually expressed by a wake function in the form of an additional term, $(\Pi/\kappa)w(y/\delta)$, added to the right-hand side of (1.1) (or (1.2)). Π is the Coles (1956) wake parameter with w assumed to be a universal function of y/δ – at least for zero-pressure-gradient flows. The complete (two-parameter) profile can then be written in defect form as

$$\frac{U_e - U}{u_\tau} = -\frac{1}{\kappa}\ln\left(\frac{y}{\delta}\right) + \frac{\Pi}{\kappa}\left(2 - w\left(\frac{y}{\delta}\right)\right), \tag{1.4}$$

independently of wall type or the specific function w chosen as the wake profile (and note that $w(1) = 2$ and $\int_0^\infty w\,\mathrm{d}(y/\delta) = 1$). Note also that in (1.4) and the expressions that follow, y and δ are to be understood as $(y - d)$ and $(\delta - d)$. Throughout this paper we employ the common definition of δ as the point where the mean velocity is 99 % of its free-stream value. In his seminal treatise on boundary layers, Rotta (1962), following Clauser (1954), defined a parameter I (Clauser's G) by

$$I = \int_0^\infty \left(\frac{U_e - U}{u_\tau}\right)^2 \mathrm{d}\left(\frac{y}{\Delta}\right), \tag{1.5}$$

where $\Delta = \delta^* U_e/u_\tau$ and δ^* is the usual displacement thickness. Employing the standard definitions for δ^* and the momentum thickness, θ, leads to

$$I = \frac{H-1}{H}\frac{U_e}{u_\tau} \equiv \frac{H-1}{H}\sqrt{\frac{2}{C_f}}, \tag{1.6}$$

where H is the usual shape parameter, δ^*/θ. I is a function only of w, Π and κ and for most wake profile shapes that have been used, can be expressed as $I = (a + b\Pi + c\Pi^2)/\kappa/(e + \Pi)$, where a, b, c and e are numerical constants whose values depend only on the specific profile shape. (For example, for the quartic polynomial wake profile suggested by Lewcowicz (1982) $I = (2.009 + 3.018\Pi + 1.486\Pi^2)/[\kappa(0.983 + \Pi)]$, compared with $I = (2 + 3.2\Pi + 1.522\Pi^2)/[\kappa(1 + \Pi)]$, which arises from Coles' profile). It also follows directly that

$$\frac{\Delta}{\delta} \equiv \frac{\delta^*}{\delta}\frac{U_e}{u_\tau} \equiv \frac{\delta^*}{\delta}\sqrt{\frac{2}{C_f}} = \frac{1+\Pi}{\kappa}. \tag{1.7}$$

Note that $H = (1 - I u_\tau/U_e)^{-1}$ and that (1.2)–(1.7) are independent of the nature of the surface and assume only that the two-parameter profile is an adequate representation of the mean flow (and, for the smooth-wall case, that the viscous sublayer can be ignored in the integrations for θ and δ). Clauser (1954) and Rotta (1962) derived the resulting relation between surface friction, $C_f \equiv 2(u_\tau/U_e)^2$, and θ. Using (1.2) rather than (1.1) to describe the log-law in the fully rough case, this relation can be re-written more conveniently as

$$\sqrt{\frac{2}{C_f}} = -\frac{1}{\kappa}\ln\left(\frac{1}{H}\sqrt{\frac{C_f}{2}}\right) + \frac{1}{\kappa}\ln\frac{\theta}{y_0} + K, \tag{1.8}$$

where $K = 2\Pi/\kappa - (1/\kappa)\ln((1+\Pi)/\kappa)$, and this can be rearranged to give

$$\frac{\theta}{y_0} = \frac{s - I}{s^2}\, \mathrm{e}^{\kappa(s-K)}, \tag{1.9}$$

where $s = \sqrt{2/C_f}$. The use of the roughness length, y_0, removes the need to consider A and ΔU^+ (in (1.1)) separately and also, as indicated above, assumes that it is determined solely by the specific roughness geometry. Notice in particular that all the above implies, quite generally, that $H = f_1(C_f, \Pi, \kappa)$ and that, for a fully rough surface, $H = f_2(\theta/y_0, \Pi, \kappa)$, $C_f = f_3(\theta/y_0, \Pi, \kappa)$. This means that given f_1, both C_f and H can be calculated as a function of θ/y_0, provided that κ is known and that Π is not dependent on the roughness type.

There is some evidence that even if a universal wake function is accepted for all kinds of boundary layers, the value of Π is significantly higher for rough-wall than for smooth-wall flows. Tani (1987), for example, re-analysed a number of previously reported data sets and found values between 0.4 and 0.75 for various types of roughness. It is difficult to obtain accurate values of Π – partly because it arises as the difference between two relatively large quantities. It is also very sensitive to the precise values chosen for the log-law constants. Recognizing the uncertainty about whether Π truly is constant, Krogstad *et al.* (1992) used a fitting procedure for the entire velocity profile (in defect form) which did not constrain Π but optimized values of u_τ, d and Π to provide the best fit (to an assumed form of the wake profile w), assuming that $\kappa = 0.41$. For their mesh roughness they found that $\Pi = 0.7$. This also led to good agreement between the optimized u_τ and the u_τ deduced from direct measurements of the turbulence shear stress. Following Perry, Lim & Henbest (1987) who were perhaps the first to demonstrate the inadequacies in standard hot-wire anemometry near rough walls, they used high-accuracy hot-wire anemometry – i.e. 120° cross-wire probes. Perry *et al.* also fitted the entire profile using Hama's (1954) inner and outer region relations and thus implicitly assumed a value for Π (about 0.51). Likewise, Bergstrom, Akinlade & Tachie (2005) made measurements over sand grain, perforated plate and wire mesh surfaces and, using a procedure similar to Krogstad's, found Π values between 0.5 and 0.65, with the highest values coming from the fully rough (rather than transitional) cases. In terms of the relationship between H and C_f given by (1.6) their data conformed well to $I = 7.0$; but this immediately implies a fixed value for Π of about 0.7 (given their wake profile shape) and a value for what they called the modified skin friction parameter, $\sqrt{C_f}(\delta/\delta^*)$, of 0.341. In proposing the latter as a 'new skin friction correlation' they appeared not to recognize that it follows directly from (1.7). Actually, they suggested a value of 0.36 ± 0.025 for this parameter which, strictly, is not consistent with their $I \equiv G = 7.0$. Note that Bergstrom *et al.* defined δ as the point at which the velocity was 99 % of the free-stream value which, as noted earlier, is the present definition.

Unlike Krogstad *et al.* (1992), the Bergstrom *et al.* work is similar to a number of previous works in the literature (e.g. those providing the data re-analysed by Tani 1987) in that no independent measurement of the wall stress was made. So its deduction, along with y_0, d and also Π (unless this is taken as known), has to come from fits of the data to the assumed two-parameter profile shape. Alternatively, if attention is concentrated on the log-law region alone, the fit has to provide C_f, y_0 and d. In either case, the process is ill-conditioned and is extremely sensitive to very small experimental uncertainties in the velocity data; this, arguably, provides one of the reasons for scatter in the values of Π, as well as uncertainty in C_f. In Hama (1954), the skin friction was determined using the momentum integral equation, by

graphical differentiation of the measured θ. In addition to the uncertainties associated with that process, even given good two-dimensionality of the flow, the mean velocity profiles were obtained using Pitot tubes without any correction for turbulence effects. This is likely to have led to significant errors, given the relatively high values of turbulence intensity near rough surfaces, particularly for cases of large h/δ. Their data thus suggest correlations noticeably different from those arising from more modern experiments, as shown later.

In the present paper, the new data sets reported were all obtained in conjunction with hot-wire and/or laser-Doppler anemometry shear stress measurements, so that C_f is known independently. The experiments cover a range of roughness types, including arrays of sharp-edged cuboid obstacles, and also include data at relatively short distances from the leading edge of the roughness, so that h/δ reached values much larger than in any previous experiments. The intention is to demonstrate that the classical formulations based on a two-parameter profile family (i.e. (1.4)–(1.8) but with a more recent wake profile shape than Coles' original) provide an adequate fit to the data over a wide range of θ/y_0, with a fixed value of $\Pi = 0.7$, and independent of the nature of the roughness geometry. The experiments are summarized in the following section, § 3 presents the results and final discussion and conclusions are given in § 4.

2. Experimental details

The data presented here were all obtained in naturally growing boundary layers, but at very different times and over very different surfaces. The early experiments, performed over 25 years ago, were undertaken in the USEPA Fluid Modelling Facility's (FMF) environmental wind tunnel, whose working section length exceeds 16 m. The roof was adjusted to ensure a zero axial pressure gradient and the rough surfaces consisted of staggered arrays of rectangular blocks 18 mm in height or, in two further cases, close-packed but sharp-edged 'sanspray' – gravel chips having typical sizes of 3 or 10 mm. The more recent experiments were undertaken over the last few years in much smaller wind tunnels at the Universities of Surrey and Southampton. These both have a working section about 4.5 m in length and 0.9 m $\times$ 0.6 m in cross-section. The surfaces consisted of a regular diamond-patterned wire mesh or staggered arrays of cubes. In the former case, the mesh wavelength was 28.6 mm and 9.7 mm in the spanwise and axial directions, respectively, with a total mesh depth of about 3 mm. The cube array surfaces comprised cubes of 5 or 10 mm in height covering 25 % of the surface in a staggered rectangular array. Figure 1 summarizes the various geometries. In each case, the roughness was mounted on baseboards which were placed on the floors of the working sections with their leading edges just downstream of the contraction exit and with suitably smooth (and short) 'lead-in' sections (ramps). In one of the cube surface cases, the (300 mm) upstream ramp was designed to 'take' the very thin boundary layer leaving the contraction exit to the top of the roughness, rather than allowing it to impact directly on the front row of roughness elements. The influence of this modification on the flow development will be discussed in due course.

Measurements were made using standard hot-wire anemometry (HWA) or, for some of the recent data, laser-Doppler anemometry (LDA). The early HWA work (at FMF) used standard single or $\pm 45^\circ$ hot-wire probes, carefully calibrated against Pitot-static probes and with on-line corrections for any drift in ambient temperature. The data have now been re-analysed, with corrections made to the near-wall shear stress measurements to account for the high turbulence intensities (using Tutu &

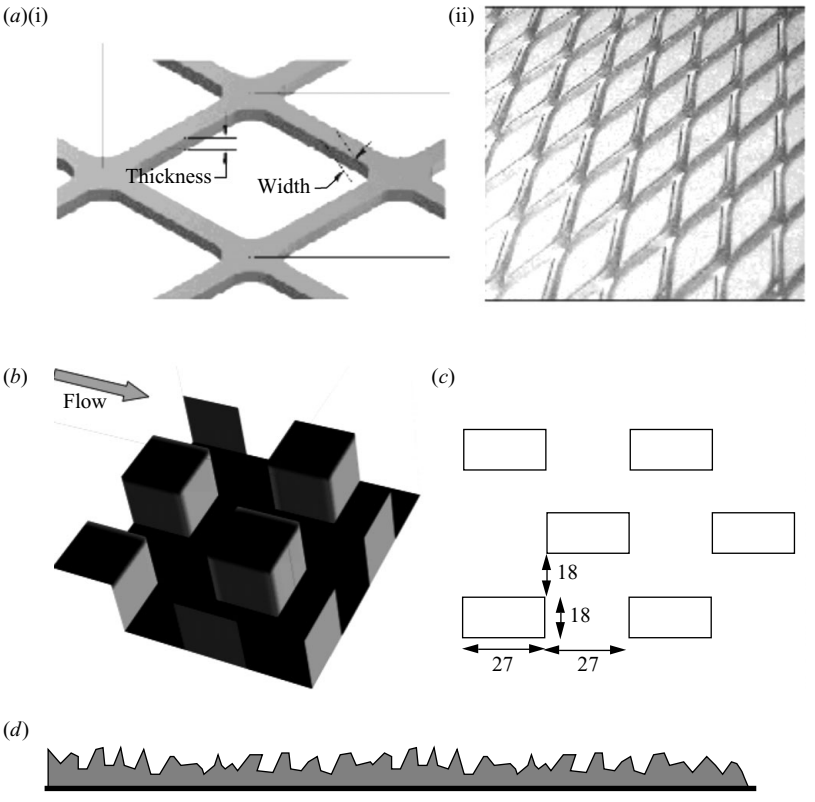

FIGURE 1. Rough surfaces used. (*a*) Mesh roughness. Flow is from bottom to top (for (i)). Thickness, axial and spanwise pitch are 3 9.7 and 28.6 mm. (*b*) Staggered cube arrays of 25 % area coverage (5 or 10 mm cubes). (*c*) FMF block roughness (25 % area coverage). Dimensions in mm (height 18). Flow from top to bottom. (*d*) FMF 'sanspray' gravel chip surfaces – average chip size 10 mm or 3 mm.

Chevray 1975). All the more recent HWA data were obtained using $\pm 60^\circ$ wires, which minimize these errors (see Perry *et al.* 1987). Data obtained with these probes, also corrected for high-turbulence effects because such corrections were not always negligible, were found to be quite close to those obtained using LDA, which provides some confidence in the accuracy of both. The probes were in all cases driven using standard CTA bridges whose outputs were filtered, amplified and digitized under the control of computers, allowing on-line calibration and measurement. Laser-Doppler anemometry data were obtained using a two-component Dantec fibre-optic probe mounted outside the tunnel. A 5 W argon-ion laser (typically operated at 1 W) was used, with the photomultiplier outputs collected and manipulated using burst spectrum analysers operating in coincidence mode. Data rates were up to 2 kHz, at least 2 min of sampling time was used at each traverse point, and transit-time data were used to provide corrections for bias errors arising from non-uniform sampling. The measurement volume was typically 2.4 mm in length (in the spanwise direction) and about 0.15 mm in diameter.

In every case, mean velocity profile data were obtained at various locations downstream of the leading edge of the roughness and at various free-stream speeds. This led to a wide range of momentum thickness Reynolds numbers ($1300 < Re_\theta < 48\,000$). Except for the FMF experiments, there was a small pressure

gradient within the working sections, arising from the boundary-layer growth on all four walls. However, this was always much smaller than that normally expected to have a measurable effect on boundary-layer flow.

3. Results

3.1. *Skin friction and shape factor correlations*

All the salient data used in the figures are given in table 1. We start by presenting skin friction and momentum thickness data. Here, C_f is defined in the usual way as the surface stress normalized by $\rho U_e^2/2$, so that $(u_\tau/U_e)^2 = C_f/2$ as in the previous section, where u_τ is by definition the wall friction velocity. This was determined by assuming that $u_\tau^2 = -\overline{uv}$, where the latter is the turbulence Reynolds shear stress measured in the near-wall region of the flow and extrapolated to $y = d$. Note that throughout this work, x and y are the axial and wall-normal directions, respectively, with the origin at the start of the roughness. There is no point in showing the many individual velocity profiles obtained during the course of all the experiments. These each have exactly the expected and well-known behaviour. We concentrate on the resulting parameters. Figure 2 shows the variation of C_f with θ/y_0, which corresponds to Re_θ for a smooth wall. θ was in every case calculated by appropriate integrations of the velocity profiles, with the very-near-surface region (between $y - d = y_0$ and the nearest measurement point) modelled using extensions to the log-law fitted to the data just above that region. The latter fits (to (1.2)) were forced to have a slope consistent with the measured $-\overline{uv}$ and with a zero-plane displacement, d, adjusted to yield the best fit. Throughout the work, we took $\kappa = 0.41$. For the reasons outlined in § 2 and because we had an independent measure of wall friction, we did not attempt to fit the entire velocity profile (with either an assumed or free value of Π) in order to determine C_f. The roughness lengths, y_0, followed directly from our fits forced to give log-law slopes consistent with the measured C_f. The fits naturally led to specific values of Π, which we discuss in due course. It is worth pointing out that although, within the roughness sublayer where the flow is spatially inhomogeneous, individual profiles are not necessarily logarithmic, it has been shown that spatially averaged mean velocities (at each height) do conform to extensions of the log-law region in the inertial layer above (Cheng & Castro 2002). So it is believed that this simple extrapolation of the velocity profile through the sublayer region is the best approach for determination of θ (and δ^*). Nonetheless, there are inevitable uncertainties in the whole process, particularly at the largest h/δ, arising largely from the uncertainties inherent in measuring the turbulence shear stress, $-\overline{uv}$, and using extrapolated values of the latter to give u_τ^2. Given the careful use of laser-Doppler anemometry and the appropriate corrections to HWA data, it is likely that u_τ errors are below $\pm 7\,\%$.

The data in figure 2 clearly collapse fairly satisfactorily for very different types of surface onto the classical result arising from a universal two-parameter profile, i.e. (1.9). Note that the latter is, in principle, dependent on the precise shape of the wake profile, through I. However, choosing, for example, either Coles' (1962) original wake function as Rotta (1962) did, or Lewkowicz's (1982) polynomial as Tani (1987) did, yields (for the same value of Π) curves which are indistinguishable above the thickness of the bold line in the figure. On the other hand, the result depends noticeably on the particular value of Π used; the bold solid line in figure 2 is the result with $\Pi = 0.7$ and it is noticeably lower than the result obtained using $\Pi = 0.55$, also shown, with the difference increasing as θ/y_0 decreases. It is also in better agreement with the experimental data. At the highest values of θ/y_0, both

Surface	x (mm)	U_e (m s^{-1})	δ (mm)	$\delta - d$ (mm)	δ^* (mm)	θ	Re_θ	θ/y_0	C_f	Π
Mesh	450	4.2	29.2	28.2	7.51	4.14	1165	25.9	0.00769	0.75
	450	8.3	29.4	28.6	7.78	4.26	2361	25.1	0.00720	0.80
	450	12.5	31.6	29.4	7.37	4.13	3447	22.9	0.00819	0.79
	450	16.8	31.5	28.8	8.00	4.40	4928	21.0	0.00845	0.55
	1000	4.3	50.0	47.5	12.3	7.07	2032	32.3	0.00770	0.70
	1000	8.8	48.7	46.3	11.4	6.46	3794	28.4	0.00700	0.83
	1000	13.2	47.5	45	11.9	6.59	5812	27.7	0.00660	0.91
	1000	17.0	48.4	45.4	12.1	6.52	7402	28.4	0.00684	0.98
	2400	4.3	95	92	22.2	13.3	3839	44.3	0.00673	0.68
	2400	8.7	89.3	81.8	20.3	12.1	7049	40.3	0.00650	0.78
	2400	13.0	91.0	88.4	21.2	12.3	10 693	29.3	0.00732	0.71
	2400	17.0	92.1	90	20.8	12.3	13 965	37.3	0.00673	0.67
	3930	18.1	123.6	121	28.7	17.1	20 634	31.1	0.00641	0.89
	3930	13.4	118	116	28.1	16.9	15 097	42.3	0.00620	0.79
	3930	8.9	117	115	27.8	16.6	9849	41.5	0.00627	0.82
	3930	4.4	114.7	113	26.8	16.2	4778	46.3	0.00620	0.78
10 mm cubes	105	10.0	32.1	22.6	6.42	3.14	2093	7.0	0.0128	0.71
	185	10.2	35.2	25.2	7.37	3.57	2380	8.5	0.0119	0.69
	345	10.3	40.4	31.4	9.61	4.86	3240	10.8	0.0101	0.78
	655	10.6	50.6	41.6	11.8	6.31	4207	15.4	0.0090	0.73
	1015	10.5	62.6	53.1	15.2	7.94	5293	14.4	0.00879	0.78
	1245	10.5	61.2	60.7	16.8	9.14	6093	16.6	0.00840	0.74
	2180	10.8	96.0	86	22.7	12.52	8347	26.1	0.00730	0.77
	3130	10.9	119.5	110	27.5	15.7	10 473	33.4	0.00680	0.73
(with high ramp)	105	10.0	29.3	21.3	5.23	2.77	1847	13.9	0.00960	0.67
	185	10.1	31.4	22.4	5.78	3.14	2093	15.7	0.00960	0.64
	345	10.2	36.2	26	7.17	3.9	2600	16.3	0.00980	0.61
	655	10.3	45.8	35.8	10.6	5.62	3747	14.8	0.00941	0.68
	1245	10.5	65.1	55.1	16.2	8.5	5667	14.7	0.00919	0.71
	2180	10.8	90.1	81.8	22.9	12.4	8233	18.5	0.00794	0.81
	3130	10.9	113.6	104.1	26.4	15.3	10 200	31.9	0.00701	0.72
5 mm cubes	432	9.6	36.5	33.0	8.63	4.53	3020	15.1	0.00840	0.81
	995	9.7	51.8	47.8	11.5	6.68	4453	26.7	0.00759	0.76
	1543	9.9	64.5	62.1	15.1	9.05	6033	34.8	0.00700	0.76
	2333	10.0	88.0	84.0	19.2	11.4	7627	45.8	0.00620	0.78
	2985	10.2	100	96.1	21.8	13.2	8800	50.8	0.00580	0.81
Rect.blocks	6000	8.0	274.1	250	54.4	32.4	29 013	43.2	0.0065	0.73
	10 000	8.0	368	350	77.6	47.7	41 387	68.1	0.00560	0.78
	12 000	8.0	416	400	88.5	54.6	47 200	78.0	0.00530	0.84
	15 000	8.0	449	430	89.6	58.0	47 787	116	0.0051	0.66
Large S-spray	6000	7.9	191.1	190	38.8	25.1	13 387	105	0.00529	0.61
	8000	7.9	236	233	47.5	31.1	16 587	156	0.00461	0.73
	10 000	7.9	287	285	57.4	37.7	20 107	151	0.00461	0.75
	12 000	7.9	350	320	62.7	42.7	22 773	251	0.00410	0.73
	15 000	7.9	385	385	72.7	50.2	26 773	279	0.00405	0.69
Fine S-spray	6000	4.0	181	180	34.8	22.6	6027	127	0.00508	0.62
	10 000	4.1	242	240	49.0	31.8	8480	212	0.00460	0.58
	12 000	4.1	290.5	290	55.1	36.6	9760	183	0.00462	0.64
	15 000	4.1	311	310	57.0	39.7	10 587	305	0.00435	0.54

TABLE 1. Salient parameter values for all profiles.

solid curves in figure 2 are close to Coles' smooth-wall line, which is here plotted on the basis that for a smooth wall, from (1.3) with $\Delta U^+ = 0$, $y_0 = (\nu/u_\tau)\,\mathrm{e}^{-\kappa A}$ so that $\theta/y_0 = 7.768\, Re_\theta \sqrt{C_f/2}$ (taking $\kappa = 0.41$, $A = 5.0$ – Coles' values). This is to be

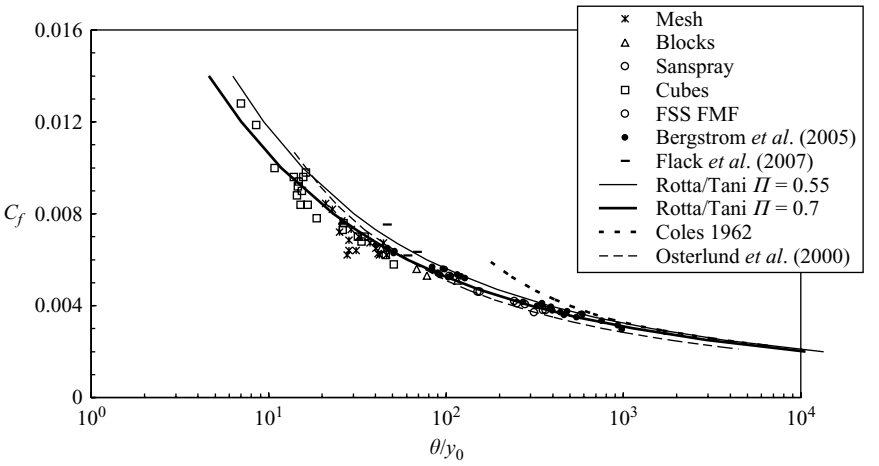

FIGURE 2. Skin friction as a function of momentum thickness.

expected, since Coles' calculated value for Π asymptotes to 0.55 at sufficiently large Re_θ (although he later adjusted it to 0.62, Coles 1987). $\theta/y_0 = 700$ corresponds, for the smooth-wall case, to Re_θ of about 2000 and for Reynolds numbers lower than this it is well known that Π falls monotonically, so the smooth-wall correlation naturally rises above the rough-wall data in that region, as seen in the figure. It is emphasized that the present rough-wall data span a wide range of Re_θ and, because of the very different types of roughness employed, the variation in Re_θ is not monotonic with θ/y_0; so in figure 2 the data point corresponding to $Re_\theta = 47\,800$ (the largest), for example, lies near $\theta/y_0 = 100$.

The figure includes the data of Bergstrom *et al.* (2005) and of Flack, Schultz & Connelly (2007), which do not extend beyond $Re_\theta = 13\,000$ in either case. It is clear that these are reasonably consistent with all the other data. (Note that for the latter set, the data have been re-analysed with the same methods as used for the present data, i.e. C_f was obtained from the LDA $\overline{uv}$ data, log-law extrapolations down to $y - d = y_0$ were used to obtain δ^* and θ, and the δ_{99} thickness was used.) It should be emphasized that some degree of scatter is inevitable because the accurate determination of y_0 is difficult. Small changes in the log-law slope (i.e. small changes in C_f) lead to large changes in y_0. It is evident that the scatter increases as θ/y_0 falls; there are various possible reasons for this. First, at this end of the θ/y_0 range, the roughness height is not very small compared to the boundary-layer height. For example, the lowest two points for the cube roughness, with $\theta/y_0 = 7 - 9$, have $h/(\delta - d) > 0.4$. With the exception of Hama's (1954) data, which suffer from the difficulties mentioned above, these are way beyond values previously studied and one would perhaps not expect close conformity to a universal velocity profile. Secondly, at such large values of h/δ, there are issues arising from the inevitable spatial inhomogeneities in the near-wall region, driven by the roughness geometry itself. These always extend above the roughness top and mean that an individual vertical profile of velocity or shear stress may not be exactly representative of the whole boundary layer at that axial location. Thirdly, this latter difficulty is exacerbated by the presence of longitudinal structures in the flow, whose spanwise wavelength is an integral multiple of the spanwise wavelength of the roughness itself. Reynolds *et al.* (2007) identified these structures in the case of cube roughness and showed that the consequent spanwise inhomogeneities

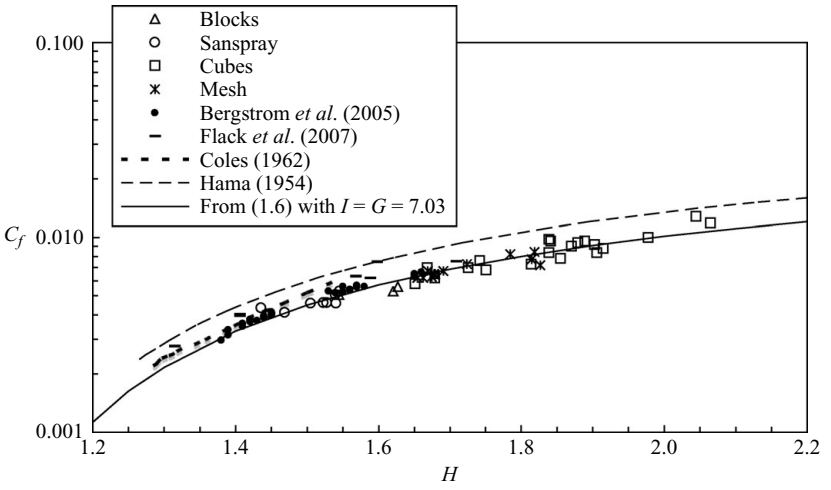

FIGURE 3. Shape factor H as a function of C_f, as predicted by (1.6), with $\Pi = 0.7$.

only fall to amplitudes similar to those present in smooth-wall boundary layers once $h/(\delta - d) < 0.05$. There is no reason to doubt that similar effects will occur for other roughness types. All these features make the deduction of C_f from turbulence shear stress data (or in any other way) rather uncertain. Indeed, for the mesh surface, for example, profiles obtained at $x = 200$ mm had a peak some way from the wall, before falling as the wall was approached. This was no doubt a result of the inevitably strong disturbance at the leading edge. Choosing this peak as a surrogate for u_τ^2 led to C_f data (having $\theta/y_0 < 10$) which was scattered by up to $\pm 20\,\%$ about the $\Pi = 0.7$ line shown in figure 2, so these data are not included.

The leading-edge disturbances could, in one sense, be considered as arising from a smooth-to-rough change of surface condition. There have been many experiments exploring the effect of roughness change on boundary-layer development (Antonia & Luxton 1971 was one of the earliest), but these have always been for cases when the upstream boundary-layer thickness (δ) is large compared with the roughness elements of the downstream surface. The results, usually couched in terms of how large a fetch is required before fully developed conditions are reached (typically around 20δ), are thus not very relevant to the present leading-edge regions, where the upstream boundary layer is very thin indeed – often smaller than the size of the roughness elements.

The relationship between C_f and H suggested by (1.6) is shown in figure 3 and overall the data are consistent with the value of I (7.03), deduced using $\Pi = 0.7$. In this case, the result is a little more sensitive to the precise wake profile shape chosen, and the curve shown assumes the Lewcowicz (1982) quartic profile (as also used by Tani 1987). The Coles' wake function (as used by Rotta) gives $I = 7.15$ with $\Pi = 0.7$, leading to a curve noticeably higher than that shown in the figure, thus having a less satisfactory fit to the data. The smoothed line through Hama's (1954) original data is included in the figure and it is evident that this is not such a good fit to the more recent data, as expected.

Figure 4 shows the extent to which all the data collapse to the result implied by (1.7) for $\sqrt{C_f/2}(\delta/\delta^*)$, which as noted earlier suggests a value of 0.34 (for $\Pi = 0.7$). It is emphasized that although there is significant scatter, fitting the velocity profiles in

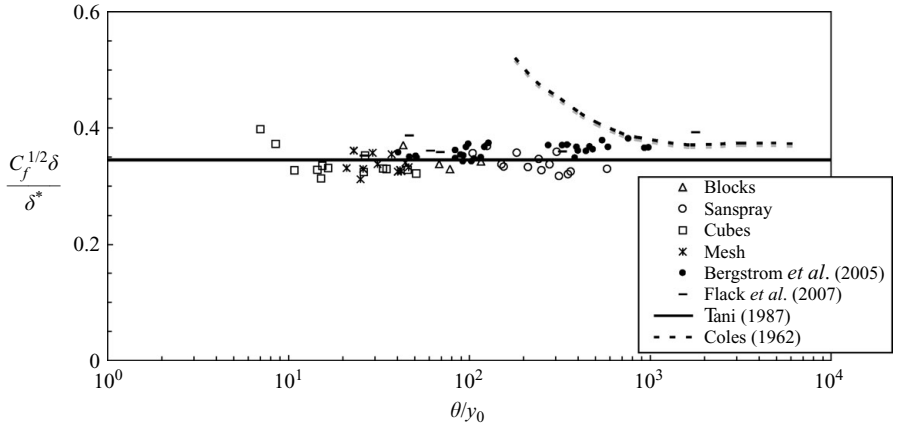

FIGURE 4. Modified skin friction, (1.7), compared with data.

a way that leaves Π as a free parameter to be determined by the fit did not, for any given roughness type, produce identifiable trends in Π with, for example, increasing θ/y_0, nor any trends between roughness types. Given the imprecise nature of such fits, as discussed earlier, we do not believe such a process has particular merit and in view of the general degree of fit between the data and the classical correlations, illustrated by figures 2–4, it would seem that the latter provide adequate descriptions of the mean flow even for 'very' rough surfaces, which might be defined as those for which $h/\delta > O(0.1)$. Notice, incidentally, the rise in $\sqrt{C_f/2}(\delta/\delta^*)$ for the smooth-wall (Coles) correlation below $\theta/y_0 \approx 1000$, in line with the falling value of Π at these low Reynolds numbers, as noted earlier.

A final remark about figures 2–4 is worth making. The 10 mm cube surface data were obtained in two cases – with and without an upstream ramp. When present, the ramp was about 300 mm in length and its surface began at $y = 0$ and finished at the top of the cubes ($y = 10$ mm). Without the ramp, there was a much more severe distortion of the very thin oncoming boundary layer, no doubt with strong separated shear layers at the first row, leading to locally larger wall stresses – and no doubt greater spatial inhomogeneity. With the ramp, these initial distortions are minimized, but the degree of scatter at small fetches is not significantly lower.

3.2. *Correlations with fetch*

It is possible to use the momentum integral equation (MIE), $\mathrm{d}\theta/\mathrm{d}x = C_f/2$, along with (1.6) and (1.9) to deduce how C_f and thus θ and δ^* will vary with fetch (x). This was done by Clauser (1954) and Rotta (1962). In a zero pressure gradient, using the present notation, the MIE yields

$$x = \int \frac{2\mathrm{d}\theta}{C_f} = \int s^2 \mathrm{d}\theta = s^2\theta - 2\int s\theta \,\mathrm{d}s. \tag{3.1}$$

There are some difficulties arising from the specification of the flow's origin, discussed in detail by Rotta. It turns out that at the origin, i.e. where $\theta = 0$, $s \equiv \sqrt{2/C_f} = I$ (and, incidentally, δ^* is strictly not equal to zero there). For a fully rough surface, (3.1) leads to a solution containing the integral exponential function, but this can be easily computed numerically, provided a value of C_f at some initial location $(x - x_0)/y_0$ is

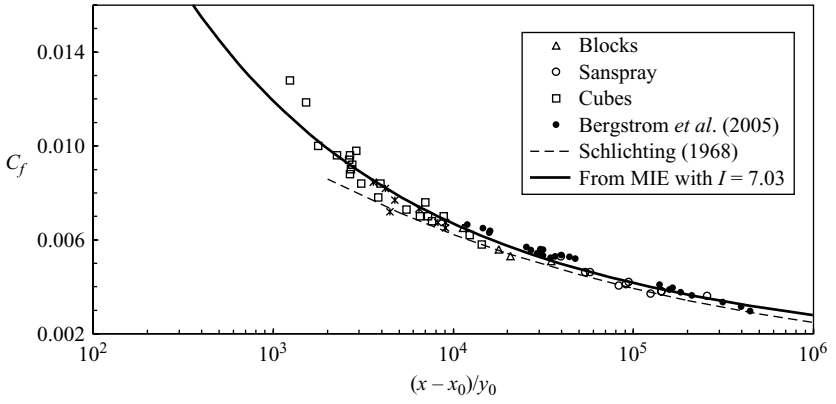

FIGURE 5. Skin friction as a function of fetch.

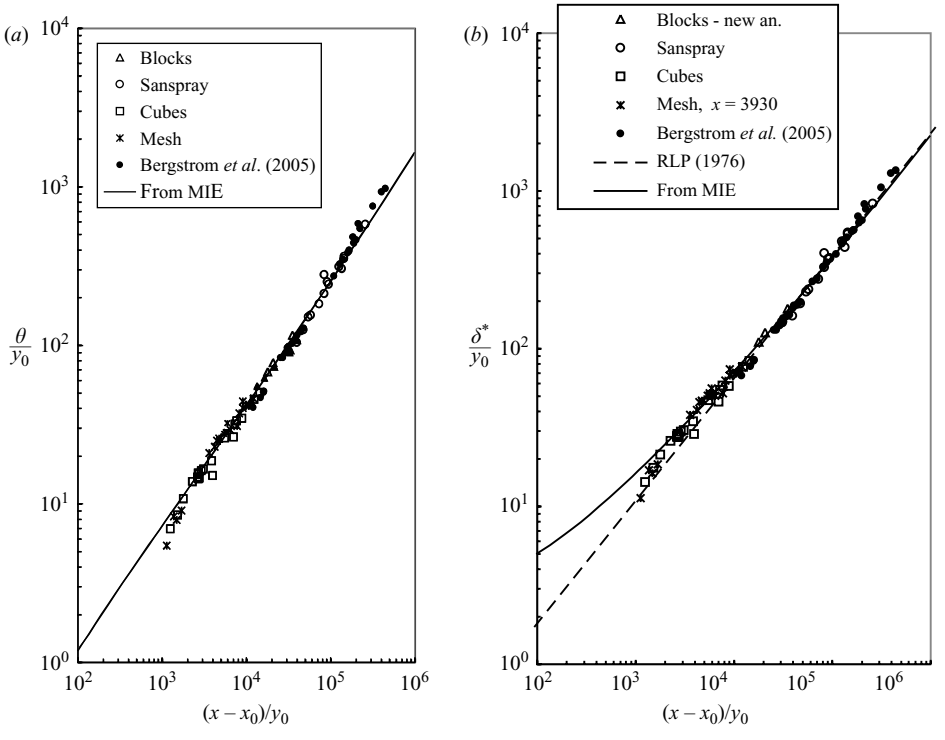

FIGURE 6. Momentum and displacement thicknesses.

specified. It seems most sensible to use $s = I$ at $x = x_0$ so that (3.1) can be written

$$x - x_0 = s^2\theta - 2\int_I^s \theta(s')s'\mathrm{d}s' \tag{3.2}$$

(and recall that θ and s are related by (1.9)). The value of x_0 was estimated for each data set by back-extrapolating a second-order polynomial fit to the θ *vs*. x data. Figure 5 shows all the data compared with the correlation calculated using (3.2). The agreement is reasonable in all cases, except for the data at the lowest fetches, in line with the results discussed previously. Figures 6(*a*) and 6(*b*) show the θ and δ^*

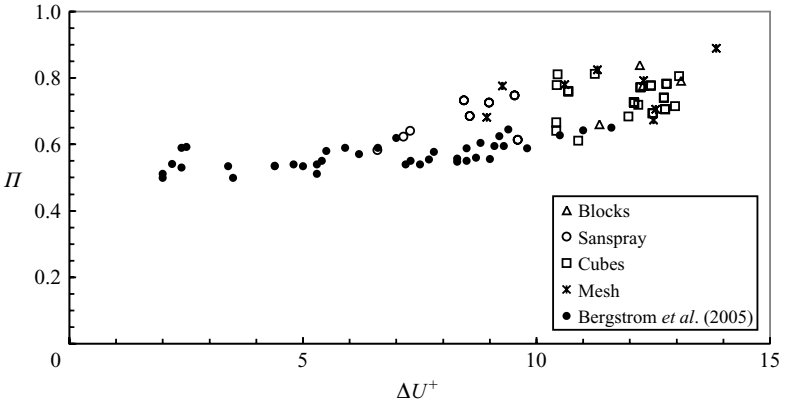

FIGURE 7. Variation of Π with roughness.

data compared with the corresponding correlations calculated from (1.9) and (1.6), respectively. Again, there is a good fit over all the range except at the lowest fetches. The data from Bergstom *et al.* (2005) have been included and these diverge noticeably at the upper end of the range, where the data are from the smallest roughness cases which, in fact, have $Re^* < 1$ and are only transitionally rough. Nonetheless, the δ^* *vs.* $(x - x_0)$ correlation is in fact very insensitive to the precise form of the profile shape (and thus to Π) and the curves shown are virtually indistinguishable from the smooth-wall equivalents. One expects transitional roughness data to collapse along with fully rough and smooth data, so the noticeably high values in Bergstrom's data must be explained another way; they are probably (at least partly) a result of uncertainties in the virtual origin, which was not measured but for the present purposes was taken as being at a distance upstream of the leading edge similar to that found typically in the present data. Figure 6(*b*) also includes Ranga Raju, Loeser & Plate's (1976) correlation, similarly covering smooth to fully rough situations. Based on Schlichting's (1968) correlations, which assumed a one-seventh power-law profile, they proposed a δ^* formulation given by

$$\frac{\delta^*}{y_0} = 0.05 \left(\frac{x - x_0}{y_0} \right)^{7/9}. \tag{3.3}$$

They were perhaps the first to suggest this kind of correlation and (3.3) is seen to be very close to the more precise result for $(x - x_0)/y_0 \gtrsim 2 \times 10^4$, but deviates noticeably at smaller fetches. To preserve clarity, their data are not included in the figure; those from the roughest of their surfaces are higher than their correlation, but fit the present more accurate one quite well.

It is worth commenting on the actual Π values which result from all the profile fits. These are shown, along with Bergstrom's data, in figure 7. Despite the not insignificant scatter which increases with roughness, as expected, there is a discernible trend of increasing Π with increasing ΔU^+, perhaps reaching values around 0.8 for the roughest surfaces. We emphasize that although the correlations included in figures 2–6 have been calculated on the basis of a fixed Π (0.7), they are mostly insensitive to the particular value used. The exceptions are figures 2 and 3 (as discussed earlier), but a change of Π to, say, 0.8 would not significantly increase the level of fit at the lowest θ/y_0 (the highest roughness). Finally, it is worth pointing out that Tani (1987) showed that Π is sensitive to initial conditions and recovers only slowly from

serious disturbances to the boundary layer. This provides yet another reason for the scatter in Π at small fetches; at these locations, one might on that basis not expect Π to have 'recovered' from the leading-edge flow. It is concluded that although there is some evidence that Π rises with roughness, the calculations made on the basis that it remains constant (at around 0.7) provide very useful correlations which fit the experimental data to within the likely accuracy of the latter. For a sufficiently large fetch, of course, θ/y_0 must eventually become so large that after a transitional region the flow would revert to a genuinely smooth-wall boundary layer, with the roughness elements well submerged within the viscous region; Π would then have the smooth-wall value (around 0.55).

3.3. *Velocity defect profiles*

Finally, it is helpful to assess the universality of the velocity profiles when plotted in deficit form. Good fits might be anticipated from the results presented earlier – recall that all the correlations have been calculated on the basis that the two-parameter family is universal, or at least sufficiently so to form the basis for obtaining useful results. Figure 8 shows a selection of data, chosen from the experiments over different surfaces and at different fetches. They are plotted using standard Rotta scaling (i.e. normalizing y by Δ, see § 1) and are compared with the Coles' universal profile (but with $\Pi = 0.7$). The profile calculated using a quartic polynomial (as used for the previous figures) is indistinguishable on the scale of these plots. Only for very small fetches, corresponding to relatively large h/δ, are there perhaps noticeable deviations – as seen for the 10 mm cube surface at $\theta/y_0 = 7$ and 8.5. There is a hint of similar behaviour for the mesh surface at $x = 0.45$ m (figure 8*f*), where $\theta/y_0 \approx 25$. One naturally expects such deviations at such low fetches. Overall, however, it is clear that there is good collapse over all surfaces, provided θ/y_0 is not too small, confirming the generally held view that mean flow deficit profiles are closely universal, independent of the type of surface.

4. Final discussion and conclusions

The major finding of the present work is that classical universality ideas adequately describe the mean flow profile of zero-pressure-gradient fully-rough boundary layers independently of the nature of the roughness or its size h with respect to the boundary-layer thickness δ, up to surprisingly large h/δ. Taking account of the zero-plane displacement d mean flow correlations calculated on the basis of the usual two-parameter profile family (log-law plus law-of-the-wake) appear to be adequate all the way up to $(h-d)/\theta = 0.5$. In particular: (i) $C_f^{1/2}\delta/\delta^* = \kappa\sqrt{2}/(1+\Pi) = 0.34 \pm 0.03$; (ii) $H = (1 - I\sqrt{C_f}/2)^{-1}$ with, for a quartic polynomial version of the wake profile, $I = 7.03$; (iii) $C_f (= 2/s^2)$ is related to θ via $\theta/y_0 = [(s-I)/s^2]e^{\kappa(s-K)}$, with $K = -0.0542$. The numerical values follow from taking $\kappa = 0.41$ and $\Pi = 0.7$. With appropriate definitions of the virtual origin of the flow, C_f, θ/y_0 and δ^*/y_0 all follow the expected variations with $(x-x_0)/y_0$ arising from integration of the momentum integral equation. The inevitable degree of scatter in the data, arising from the uncertainties in obtaining C_f and H with high accuracy, is insufficient to mask a probable slow rise in the wake parameter Π with increasing roughness, characterized by Re^* or equivalently ΔU^+. However, the changes are not really large enough to warrant attempts to refine the correlations by allowing Π to vary (from 0.7); we argue that the above correlations may be taken as useful practical guides, appropriate for any type of fully rough

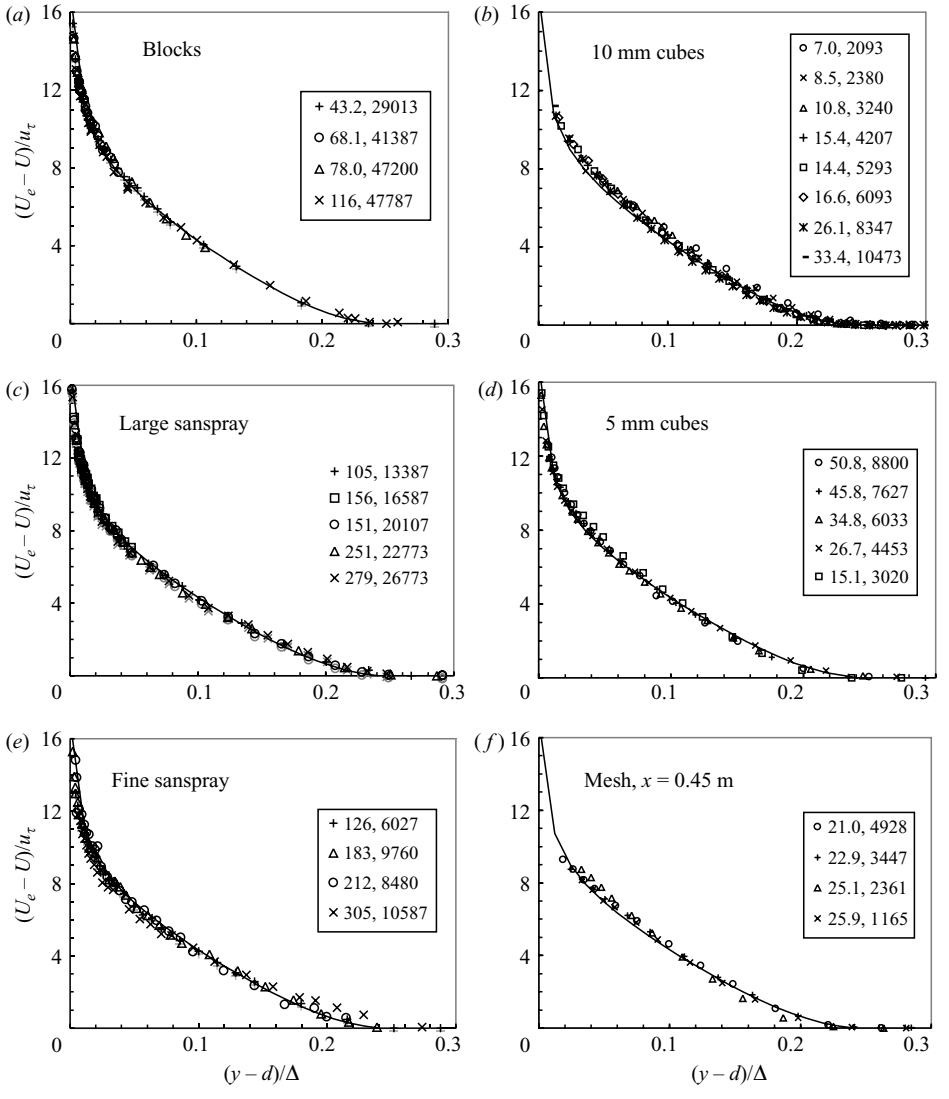

FIGURE 8. Deficit velocity profiles. Surface type is indicated on each figure, with the keys giving values of (first) θ/y_0 and Re_θ. The solid line in each figure is the Coles profile (with $\Pi = 0.7$).

surface. It would also be impractical to attempt to identify specific values of Π for specific roughness types.

The issue of how the mean flow profile could be parameterized for what may be termed extremely rough-wall boundary layers – i.e. once $(h - d)/\theta > 0.5$ or, equivalently, $h/\delta > 0.2$ – has not been addressed here. It is certainly the case that the profiles will be very dependent on the immediate history of the flow and the detailed geometry of the roughness. As noted by Jiménez (2004), one might then more profitably consider the situation as that of a uniform flow over a collection of discrete bluff bodies, rather than an identifiable two-dimensional boundary layer, and it is probably not sensible to expect any kind of universality. What is clear from the present work, however, is that classical universality remains useful over a much wider

range of θ/y_0 than often thought. We have also not addressed the issues surrounding possible differences in the turbulence structure (especially in the outer flow) as θ/y_0 rises. The turbulence data collected during the course of this work show, perhaps not surprisingly, that this changes significantly at values of θ/y_0 significantly higher than those for which mean flow universality first breaks down. Despite an increasing literature on the topic, there is as yet little consensus about either the extent or the nature of these changes, and the issue requires more attention.

Numerous colleagues have been involved with the author in undertaking the experiments to obtain the raw data. These are principally Dr W. H. Snyder and Mr R. E. Lawson (Fluid Modelling Facility, USEPA, retired), Dr H. Cheng, Dr P. Hayden and Mr T. Lawton (EnFlo, University of Surrey) and Dr H. C. Lim and Miss S. Merritt (University of Southampton). The author is very grateful to them all and emphasizes that they should not be held culpable for the data analysis and accompanying thoughts contained herein. Thanks are also due to the referees for some helpful suggestions, to the Engineering and Physical Sciences Research Council who supported some of the more recent work through Grant EP/D036771, and to the Natural Environment Research Council who also supported some of the work through the UWERN Grant DST/26/39.

REFERENCES

Acharya, M., Bornstein, J. & Escudier, M. P. 1986 Turbulent boundary layers on rough surfaces. *Exps. Fluids* **4**, 33–47.

Antonia, R. A. & Luxton, R. E. 1971 The response of a turbulent boundary layer to a step change in surface roughness. *J. Fluid Mech.* **48**, 721–761.

Bergstrom, D. J., Akinlade, O. G. & Tachie, M. F. 2005 Skin friction correlation for smooth and rough wall turbulent boundary layers. *Trans. ASMEI: J. Fluids Engng* **127**, 1146–1153.

Cheng, H. & Castro, I. P. 2002 Near-wall flow over urban-type roughness. *Boundary Layer Met.* **104**, 229–259.

Clauser, F. H. 1954 Turbulent boundary layers in adverse pressure gradients. *J. Aeronaut. Sci.* **21**, 91–108.

Coles, D. E. 1956 The law of the wake in the turbulent boundary layer. *J. Fluid Mech.* **1**, 191–226.

Coles, D. E. 1962 The turbulent boundary layer in a compressible fluid. *USAF Rep.* R-403-PR.

Coles, D. E. 1987 Coherent structures in turbulent boundary layers. In *Perspectives in Turbulence Studies* (ed. H. U. Meier & P. Bradshaw), pp. 93–114. Springer.

Flack, K., Schultz, M. S. & Connelly, J. S. 2007 Examination of a critical roughness height for outer layer similarity. *Phys. Fluids.* (in press).

Granville, P. S. 1987 Three indirect methods for the drag characterisation of arbitrarily rough surfaces on flat plates. *J. Ship Res.* **31**, 70–77.

Hama, F. R. 1954 Boundary-layer characteristics for smooth and rough surfaces. *Trans. Soc. Nav. Arch. Mar. Engrs* **62**, 333–351.

Jackson, P. S. 1981 On the displacement height in the logarithmic velocity profile. *J. Fluid Mech.* **111**, 15–25.

Jiménez, J. 2004 Turbulent flows over rough walls. *Annu. Rev. Fluid Mech.* **36**, 173–196.

Krogstad, P.-A., Antonia, R. A. & Browne, L. W. B. 1992 Comparison between rough- and smooth-wall turbulent boundary layers. *J. Fluid Mech.* **245**, 599–617.

Lewcowicz, A. K. 1982 An improved universal wake function for turbulent boundary layers and some of its consequences. *Z. Flugwiss. Weltraumforschung* **6**, 261–266.

Mills, A. F. & Hang, X. 1983 On the skin friction coefficient for a fully rough plate. *Trans. ASMEI: J. Fluids Engng* **105**, 364–365.

Österlund, J. M., Johansson, A. V., Nagib, H. M. & Hites, M. H. 2000 A note on the overlap region in turbulent boundary layers. *Phys. Fluids* **12**, 1–4.

Perry, A. E., Lim, K. L. & Henbest, S. M. 1987 An experimental study of the turbulence structure in smooth and rough wall turbulent boundary layers. *J. Fluid Mech.* **177**, 437–466.

Ranga Raju, K. G., Loeser, J. & Plate, E. J. 1976 Velocity profiles and fence drag for a turbulent boundary layer along smooth and rough plates. *J. Fluid Mech.* **76**, 383–399.

Raupach, M. R., Antonia, R. A. & Rajagopalan, S. 1991 Rough-wall turbulent boundary layers. *Appl. Mech. Rev.* **44**, 1–25.

Reynolds, R. T., Hayden, P., Castro, I. P. & Robins, A. G. 2007 Spanwise variations in nominally two-dimensional rough-wall boundary layers. *Exps. Fluids* (in press).

Rotta, J. C. 1962 The calculation of the turbulent boundary layer. *Prog. Aeronaut. Sci.* **2**, 1–219.

Schlichting, H. 1968 *Boundary Layer Theory*, 6th edn. McGraw–Hill.

Snyder, W. H. & Castro, I. P. 2002 The critical Reynolds number for rough-wall boundary layers. *J. Wind Engng Indust. Aerodyn.* **90**, 41–54.

Tani, I. 1987 Turbulent boundary layer development over rough surfaces. *Perspectives in Turbulence Studies* (ed. H. U. Meier & P. Bradshaw), pp. 223–249. Springer.

Tutu, N. & Chevray, R. 1975 Cross-wire anemometry in high-intensity turbulence. *J. Fluid Mech.* **71**, 785–800.

Townsend, A. A. 1976 *The Structure of Turbulent Shear Flow*, 2nd edn. Cambridge University Press.